*Korean J. Chem. Eng.*, 34(7), 1936-1943 (2017)
DOI: 10.1007/s11814-017-0107-0

pISSN: 0256-1115
eISSN: 1975-7220

# Effect of oxidation states of Mn in $Ca_{1-x}Li_xMnO_3$ on chemical-looping combustion reactions

**Byeong Sub Kwak*, No-Kuk Park**, Jeom-In Baek***, Ho-Jung Ryu****, and Misook Kang*,†**

*Department of Chemistry, College of Science, Yeungnam University, Gyeongsan, Gyeongbuk 38541, Korea
**School of Chemical Engineering, Yeungnam University, Gyeongsan, Gyeongbuk 38541, Korea
***Korea Electric Power Corporation Research Institute, 105 Munji-ro, Yuseong-gu, Daejeon 34056, Korea
****Korea Institute of Energy Research, 152 Gajeong-ro, Yuseong-gu, Daejeon 34129, Korea
(*Received 18 January 2017 • accepted 10 April 2017*)

**Abstract**−We investigated the effect of the oxidation state of Mn in $CaMnO_3$ perovskite particles to improve their oxygen transfer performance for chemical-looping combustion (CLC). Li was introduced in the Ca site of $CaMnO_3$ to increase the Mn oxidation state. $Ca_{1-x}Li_xMnO_3$ particles were synthesized by the solid-state method, and the amount of Li added ranged from 0 to 0.015 mol. The structure of the synthesized $Ca_{1-x}Li_xMnO_3$ particles was examined using XRD, and all particles were confirmed to have a $CaMnO_3$ perovskite structure. The shape and chemical properties of the prepared particles were characterized by using SEM and $CH_4$-TPD. The binding energy and oxidation state of the different elements in the $Ca_{1-x}Li_xMnO_3$ particles were measured by XPS. When Li was added, the oxidation state of Mn in $Ca_{1-x}Li_xMnO_3$ was higher than that of Mn in $CaMnO_3$. The oxygen transfer performance of the particles was determined by an isothermal $H_2$-$N_2$/air and $CH_4$-$CO_2$/air redox cycle at 850 °C, repeated ten times, using TGA. All particles showed an oxygen transfer capacity of about 8.0 to 9.0 wt%. Among them, $Ca_{0.99}Li_{0.01}MnO_3$ particles had the best performance and the oxygen transfer capacity under $H_2$-$N_2$/air and $CH_4$-$CO_2$/air atmosphere was 8.47 and 8.75 wt%, respectively.

Keywords: Chemical Looping Combustion, Oxygen Carrier, Perovskite, $CaMnO_3$, Li Promoter

## INTRODUCTION

$CO_2$ emissions have increased due to industrialization and the use of fossil fuels, both of which have accelerated global warming. If the rate of global warming continues to increase, plants, animals, and humankind will be profoundly impacted. Therefore, many researchers have been working to reduce $CO_2$ emissions to delay this problem. However, within the present industrial structure, it is difficult to significantly reduce $CO_2$ emissions. A more feasible solution is to capture and store the generated $CO_2$, or convert it to a useful compound. There are three technologies aimed to capture $CO_2$. These technologies are divided according to their approach as pre-combustion [1,2], oxy-fuel combustion [3,4], and post-combustion [5,6]. Specifically, among the oxy-fuel combustions, chemical looping combustions (CLC) can supply pure oxygen to the fuel; therefore, they do not generate NOx, and no separation equipment is required [7]. The reaction system is shown in Fig. 1, and the mechanism is given by Eq. (1) and (2) [8,9].

$$\text{FR: } (2n+m/2)M_xO_y+C_nH_m \rightarrow (2n+m/2)M_xO_{y-1}+nCO_2+m/2H_2O \quad (1)$$

$$\text{AR: } 2M_xO_{y-1}+O_2 \rightarrow 2M_xO_y \quad (2)$$

The reaction system consists of a fuel reactor (FR) and an air reactor (AR). The fuel reactor receives oxygen from a metal oxide, which acts as the oxygen carrier. This oxygen is then converted to $CO_2$ and $H_2O$, and the metal oxide is reduced to a metal. The reduced oxygen carrier particles move to the air reactor (AR) and are regenerated with the metal oxide by reacting with oxygen in the air. As can be seen from the mechanism of this reaction, the oxygen transfer performance of the metal oxides as oxygen carriers is very important. The main metal oxides used as oxygen carriers are $Mn_3O_4$ [10], $Fe_2O_3$ [11], $Co_2O_3$ [12], NiO [13,14], and CuO [15]. Among them, even though $Fe_2O_3$, $Co_3O_4$, NiO, and CuO show an

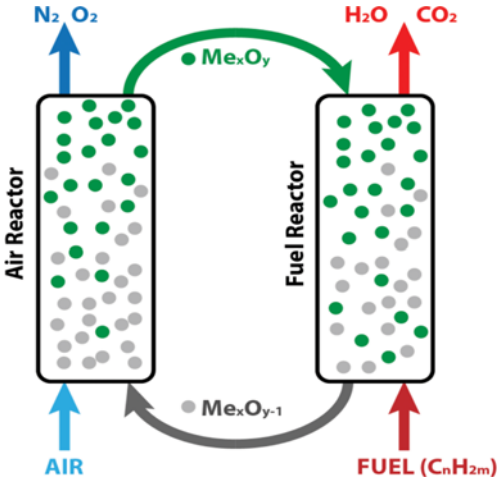


**Fig. 1. Schematic view of chemical looping combustion.**

†To whom correspondence should be addressed.
E-mail: mskang@ynu.ac.kr

initially high performance, when the redox cycle is repeated, deactivation rapidly occurs because of the aggregation of the particles with each other. To solve this problem, MgO [16], $Al_2O_3$ [17], $MgAl_2O_4$ [18], $SiO_2$ [19], $TiO_2$ [20], and $ZrO_2$ [21] are used as supports. However, these supports are difficult to reduce owing to their low reduction potential. Therefore, a decrease in the overall oxygen transfer performance is inevitable when using the supports.

Further, although the redox cycle using $Mn_3O_4$ is repeated, the deactivation due to aggregation is not shown. Because $Mn_3O_4$ is composed of $MnO{\cdot}Mn_2O_3$, Mn exists as $2^+$ and $3^+$ ions, and the reduction potential of these ions is as follows:

$$Mn^{3+}+e^- \leftrightarrow Mn^{2+} \qquad E^o=1.56\ eV \qquad (3)$$

$$Mn^{2+}+2e^- \leftrightarrow Mn_{(s)} \qquad E^o=-1.18\ eV \qquad (4)$$

According to the reduction potential, although the $Mn^{3+}$ ion is easily reduced to $Mn^{2+}$, it is difficult to reduce the $Mn^{2+}$ ion to $Mn_{(s)}$. Therefore, the reduction from manganese oxide to metallic Mn is difficult, and this is the reason why the aggregation does not occur on the manganese oxide oxygen carrier particles. However, this property causes an approximately 6.9 wt% lower oxygen transfer performance than other transition metal oxide particles. To improve the performance of manganese oxide particles, the oxidation state of the Mn ion in the structure should be increased to $4^+$, $6^+$, or $7^+$.

In $KMnO_4$, the oxidation state of Mn ion is $7^+$. However, this material cannot be used for CLC as an oxygen carrier particle because its melting point is 240 °C, which is rather low. Sodium and lithium can replace potassium; however, sodium cannot be used because $Na_2O$ also has a low melting point of 1,132 °C, which is similar to the reaction temperature. Thus, $LiMnO_x$ was synthesized using $Li_2O$, which has a melting point of 1,438 °C, and subsequent studies were carried out. The initial oxygen transfer performance of the $LiMnO_x$ particles was 9.11 wt%, which is a value higher than that of $Mn_3O_4$; however, as the reaction continued, it decreased to 6.88 wt%, and the reaction rate was also very slow. Therefore, these compounds were considered to be improper oxygen carrier particles.

Other usable candidate materials include perovskites, with the $ABO_3$ general formula. The A and B metal oxidation state of perovskites are $2^+$ and $4^+$, respectively. Manganese is located in the B site, and an alkaline earth metal is used in the A site. $CaMnO_{3-\delta}$ [22], $CaMn_{1-x}B_xO_{3-\delta}$ (B=Al, V, Fe, Co, and Ni) [23], $Ca_{1-x}A_xMnO_3$ (A=Sr and Ba) [24], and $CaMg_{0.1}Ti_{0.125}Mn_{0.775}O_{2.9-\delta}$ [25] have been studied and reported. These reported particles have shown an excellent performance, but the oxidation state of Mn is based on $4^+$. Therefore, the present study aimed to improve the oxygen transfer performance of particles by increasing the oxidation state of Mn to a value higher than $4^+$. To increase the oxidation state of Mn, $Ca_{1-x}Li_xMnO_3$ was synthesized with a substitution of Li in the Ca sites and evaluated for CLC. The particles were synthesized by the solid-state method, and their oxygen transfer performance was tested under $H_2$ and $CH_4$ atmospheres using a TGA.

## EXPERIMENTAL

### 1. Preparation of $Ca_{1-x}Li_xMnO_3$ Particles

In this study, $Ca_{1-x}Li_xMnO_3$ perovskites were prepared using a solid-state method, and the prepared particles were labeled as X=0, 0.005, 0.01, and 0.015 according to the added Li ratio. Calcium hydroxide ($Ca(OH)_2$, Shinyo pure chemical Co., LTD, Japan), lithium hydroxide monohydrate ($LiOH{\cdot}H_2O$, Junsei chemical Co., LTD, Japan), and manganese dioxide ($MnO_2$, Duksan pure Co., LTD, Republic of Korea) were used as precursors. The precursors were homogeneously mixed by using a mortar and pestle for 1 hour. Thereafter, the mixed powders were pelletized and heated at 1,300 °C for 10 h to bring about their crystallization. The particles were then broken and sieved to 45-180 μm.

### 2. Characterization

The structure of the prepared particles was determined through powder X-ray diffraction (XRD, model MPD from PANalytical) using a nickel-filtered CuK$\alpha$ radiation (40.0 kV, 30.0 mA) source, at 2-theta angles from 10 to 80°. The shapes of the particles were examined by a scanning electron microscope (SEM, S-4100, Hitachi, LTD, Japan) operated at 15 kV. The particles' surface area was measured with a Belsorp II instrument (BEL, Japan). $CH_4$-TPD (Temperature programmed desorption) experiments were conducted using a BELCAT (BEL, Japan) to confirm the adsorption ability of the particles. To remove the water and impurities on the surface of the particles, the obtained particles were first pretreated under a He atmosphere at 500 °C for 1 h. Then, $CH_4$ (5 vol% $CH_4$/He) gas flowed into the reactor for 1 h at 50 °C. Subsequently, He was introduced at 50 °C for 15 min to remove the physisorbed $CH_4$. Finally, the CH4-TPD experiments were conducted by increasing the temperature from 50 to 1,000 °C, at a rate of 10 °C $min^{-1}$, under He flow. X-ray photoelectron spectroscopy (XPS, K-alpha, Thermo Scientific, UK), using Al K$\alpha$ (1,486.6 eV) X-rays as the excitation source, was carried out to investigate the binding energies of Li 1s, Ca 2p, Mn 2p, and O 1s. Prior to their measurement, the particles were stored under vacuum ($1.0\times10^{-7}$ Pa) overnight to remove the water from their surface. The base pressure system was less than $1\times10^{-9}$ Pa. The obtained signals were fitted by using mixed Lorentzian-Gaussian curves.

### 3. Measurement of Redox Activity Cycles

Fig. 2 shows a schematic diagram of the reaction conditions for the reduction-oxidation (redox) cycle test. The reactivity of the syn-

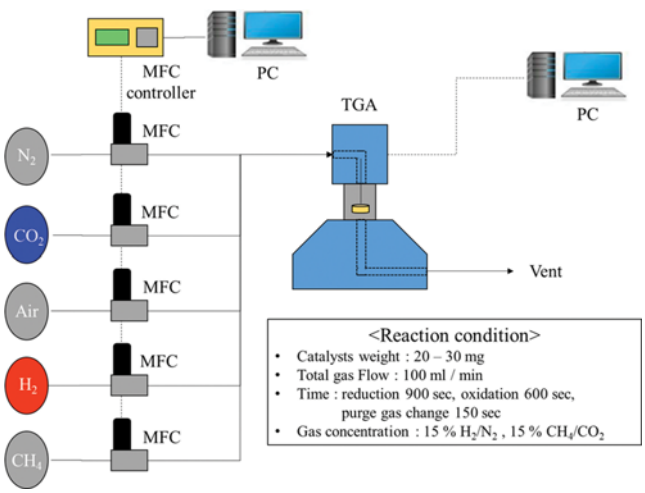


**Fig. 2. Schematic of experimental set up for redox cycle.**

thesized particles was evaluated using a thermogravimetric analyzer (TGA, Shinco co, Republic of Korea). About 20 to 30 mg of the particles were loaded into an alumina container, which was then placed in the furnace of the TGA. The furnace was then filled with $N_2$, and the temperature was raised to 850 °C. Following this, $H_2$ (15 vol% $H_2/N_2$) or $CH_4$ (15 vol% $CH_4/CO_2$) was used as fuel for the reduction reaction, and air was used for the oxidation reaction. All of the gases were kept at a constant flow of 100 mL/min. The reaction time of the reduction and oxidation was 900 s and 600 s, respectively. After the oxidation and reduction reactions, a flow of $N_2$ or $CO_2$ was introduced for 150 s to prevent any mixing between the fuel and air. These redox cycles were conducted ten times. The oxygen carrier capacity of the particles was calculated as follows:

$$Ro=[m_{ox}-m_{red}]/m_{ox} \quad (5)$$

## RESULTS AND DISCUSSION

The XRD patterns of the $Ca_{1-x}Li_xMnO_3$ particles are shown in Fig. 3. For all particles, peaks were observed at $2\theta$=23.600, 33.672, 41.600, 48.495, 60.423, 71.101, and 81.135° and assigned to the (101),

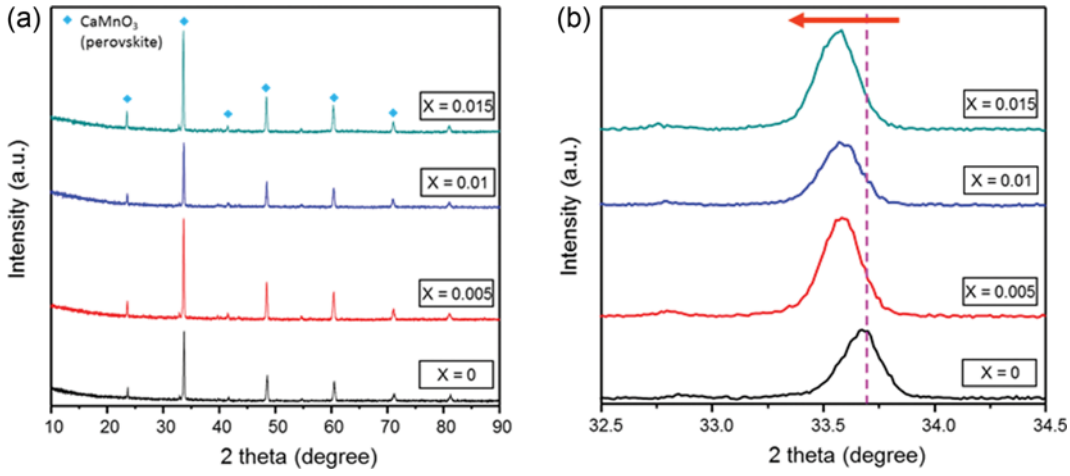


**Fig. 3. The (a) XRD patterns and (b) enlarged view of (121) plane of the $Ca_{1-x}Li_xMnO_3$ particles.**

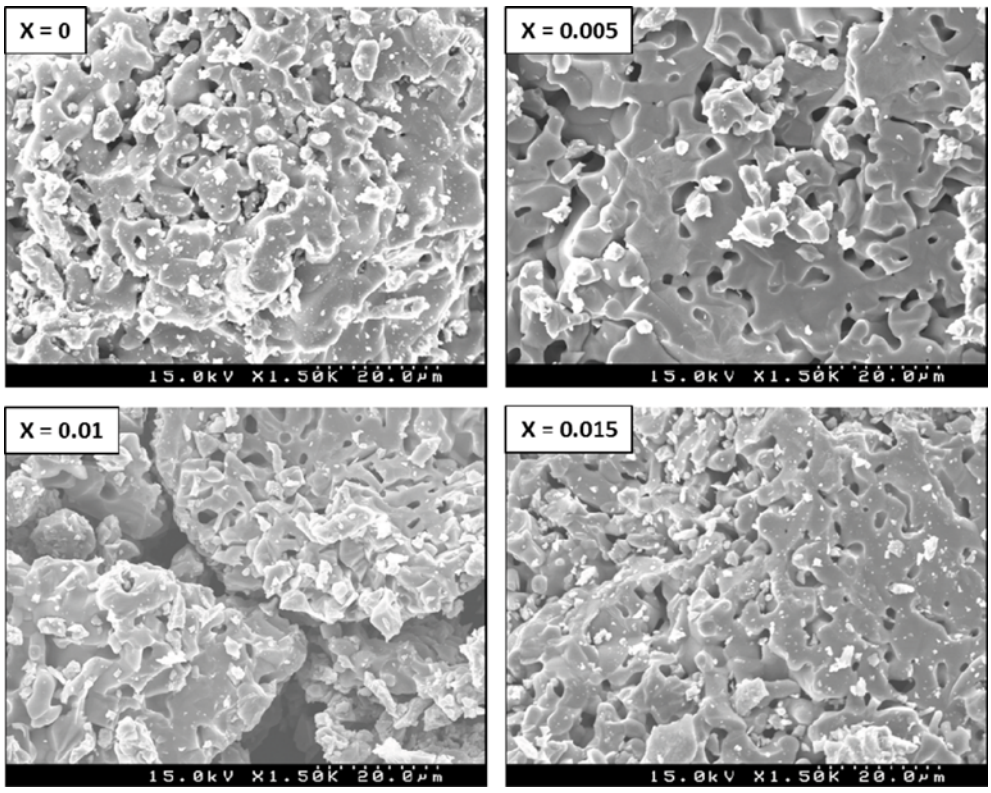


**Fig. 4. The SEM images of the $Ca_{1-x}Li_xMnO_3$ particles.**

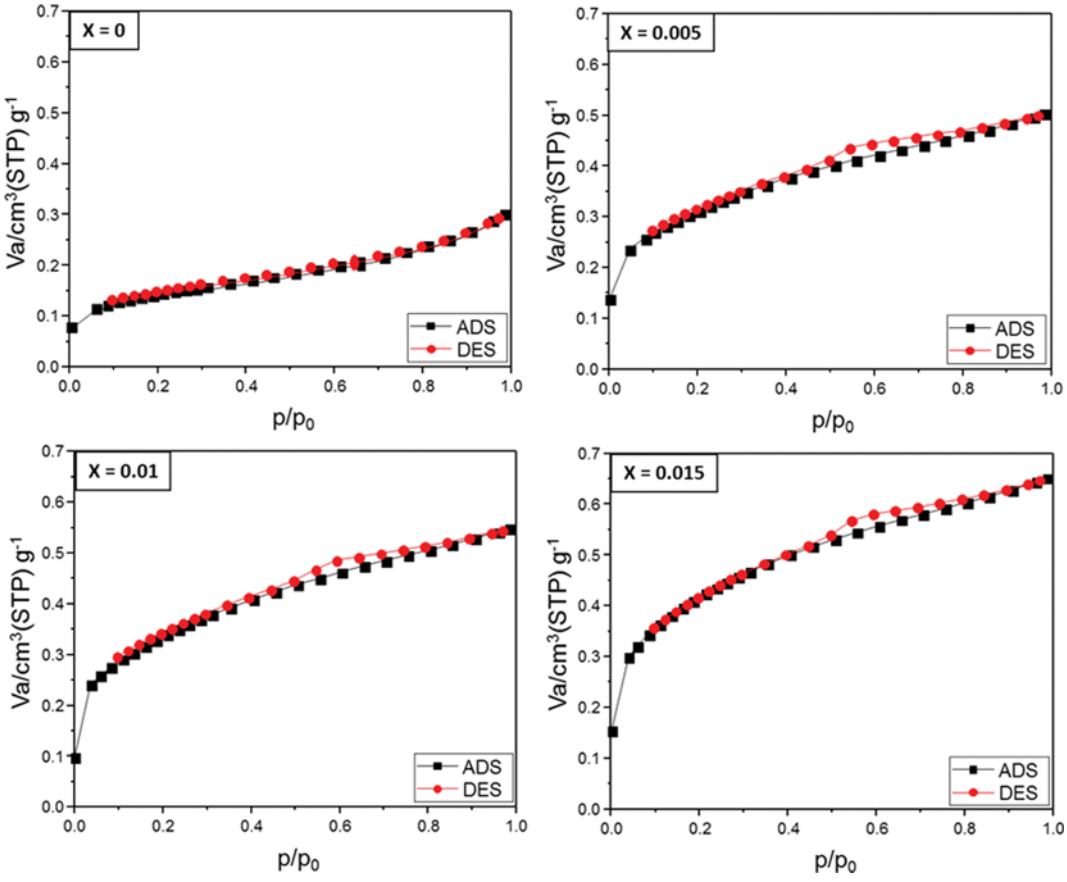


**Fig. 5. $N_2$ adsorption-desorption isotherm curves at 77 K for the $Ca_{1-x}Li_xMnO_3$ particles.**

**Table 1. The atomic % by XPS and surface area induced by N2 adsorption-desoroption isotherm curves for $Ca_{1-x}Li_xMnO_3$ particles**

(Atomic %)

| Particle | Li 1s | Ca 2p | Mn 2p | O 1s | Specific surface area ($m^2g^{-1}$) |
|---|---|---|---|---|---|
| $CaMnO_3$ | - | 24.959 | 24.661 | 50.405 | 0.1900 |
| $Li_{0.005}Ca_{0.995}MnO_3$ | 2.472 | 25.704 | 25.687 | 46.201 | 0.5040 |
| $Li_{0.01}Ca_{0.99}MnO_3$ | 3.015 | 25.052 | 25.699 | 46.134 | 1.3077 |
| $Li_{0.015}Ca_{0.985}MnO_3$ | 3.789 | 24.097 | 27.773 | 44.340 | 1.4311 |

(121), (022), (202), (123), (242), and (204) planes, respectively, of $CaMnO_3$ perovskite (JCPDS 98-101-8097). Although up to 0.015 mol of Li was used to replace the Ca site, the XRD results do not show any structural changes. According to the XRD results, it is considered that the added Li was well substituted at the Ca site. However, it was confirmed that the XRD peaks were shifted to the lower angle as Li was added. This is because the $CaMnO_3$ perovskite structure is distorted by the addition of Li. The structure distortion can affect the oxidation state and oxygen mobility of the lattice.

Fig. 4 shows SEM images of the surfaces of the particles. The surface of the $CaMnO_3$ particles was observed to be smooth and dense. However, as the amount of added Li increased, the pore on the surface of the particles increased gradually. These observations suggest that the oxygen transfer performance of the particles can be increased owing to the high surface area that comes in contact with the feed gases.

Fig. 5 shows the $N_2$ adsorption-desorption isotherm curves at 77 K of the particles. All the isotherm curves showed II type, which were identified as non-porous according to the IUPAC classification. However, the specific surface area of the particles in Table 1 was increased as the addition amount of Li is increased. This result appears to be due to the increased porosity as shown in the SEM image. These results lead to an increase in the area of contact with the feed gases. Therefore, the reaction performance of the particles can be improved.

The $CH_4$ absorption ability of the oxygen carrier particle is an important factor during CLC reactions because $CH_4$ is used as the feed gas. The $CH_4$-TPD profiles of the $Ca_{1-x}Li_xMnO_3$ particles are shown in Fig. 6. Methane desorption peaks were widely observed from 600 °C to 1,000 °C, and the highest peaks were discovered at about 850 °C to 950 °C. Even though desorption peaks were ob-

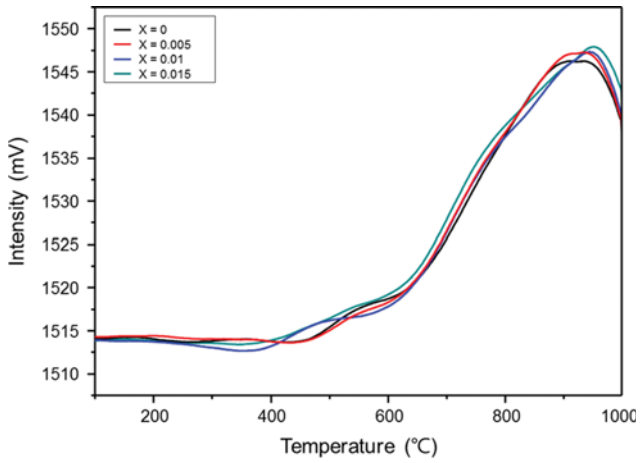


**Fig. 6. The $CH_4$-TPD profiles for the $Ca_{1-x}Li_xMnO_3$ particles.**

served at similar temperatures in every particle, because the basic composition of the particles is not significantly different, as up to 0.015 mol of Li were added, the desorption peaks shifted to a higher temperature. This result means that the interaction between the particle's surface and $CH_4$ increased, which is considered to be an advantage in CLC reactions carried out under $CH_4$ flow.

Fig. 7 shows the results of the redox cycle tests, which were repeated ten times under a $H_2$-$N_2$/air or $CH_4$-$CO_2$/air atmosphere, at 850 °C. It was confirmed that the redox cycle reaction was stable in both the $H_2$-$N_2$/air and $CH_4$-$CO_2$/air atmospheres, and that the oxygen transfer capacity was about 8.0 to 9.0 wt% in all particles. In the $H_2$-$N_2$/air atmosphere, the oxygen transfer capacity of $CaMnO_3$, X=0.005, 0.01, and 0.015 was 8.25, 8.27, 8.47, and 8.29 wt%, respectively, as can be observed in Fig. 7(a) and (b). Similarly, the oxygen transfer capacity of $CaMnO_3$, X=0.005, 0.01, and 0.015 in the $CH_4$-$CO_2$/air atmosphere was 8.29, 8.45, 8.75, and 8.44 wt%, respectively, as presented in Fig. 7(c) and (d). The reaction results show that the oxygen transfer capacity improved when up to 0.01 mol of Li was used to replace Ca. However, a performance decrease was revealed when the Li amount was increased to more than 0.01 mol. These results suggest that a small amount of Li substitution helps increase the oxidation state of Mn. However, when a large amount of Li was used, it induced the formation of $LiMnO_x$ in the $Ca_{1-x}Li_xMnO_3$ structure, and the performance of the material decreased.

To study the conversion versus oxygen transfer rate for the reduction and oxidation for the $Ca_{1-x}Li_xMnO_3$ particles, the redox cycle results were used to calculate the normalized conversion and oxygen transfer rates of the particles, as follows: [26]

$$\text{Reduction conversion: } X_{red}=[m_{ox}-m]/[m_{ox}-m_{red}] \quad (6)$$

$$\text{Oxidation conversion: } X_{red}=1-[m_{ox}-m]/[m_{ox}-m_{red}] \quad (7)$$

$$\text{Oxygen transfer rate: } r_{O_2}=Ro\cdot dX/dt \quad (8)$$

The determined results are presented in Fig. 8. The reaction rate of the oxidation was faster than the reduction rate, and the reduction rate in the $CH_4$ atmosphere was about twice as fast as that in the $H_2$ atmosphere. In the $H_2$ atmosphere, a constant rate of about 15 μmol $O_2/g_{oc}$ was observed because the supply of $H_2$, which can receive $O_2$, was consistent. On the other hand, in the $CH_4$ atmosphere, the rate increased from when $CH_4$ decomposed,

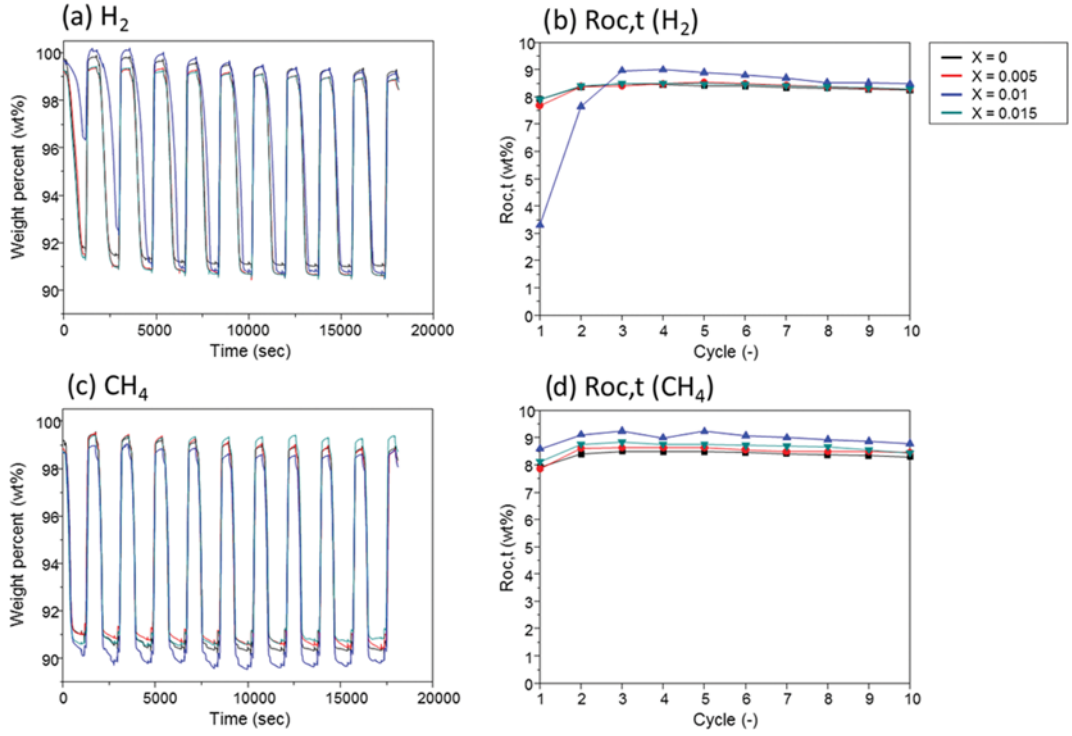


**Fig. 7. The cyclic redox ((a) and (c)) and Roc,t ((b) and (d)) on the $Ca_{1-x}Li_xMnO_3$ particles in TGA at 850 °C. Condition: (a) and (b) $H_2$ (15 vol% $H_2/N_2$)/air, (c) and (d) $CH_4$ (15 vol% $CH_4/CO_2$)/air.**

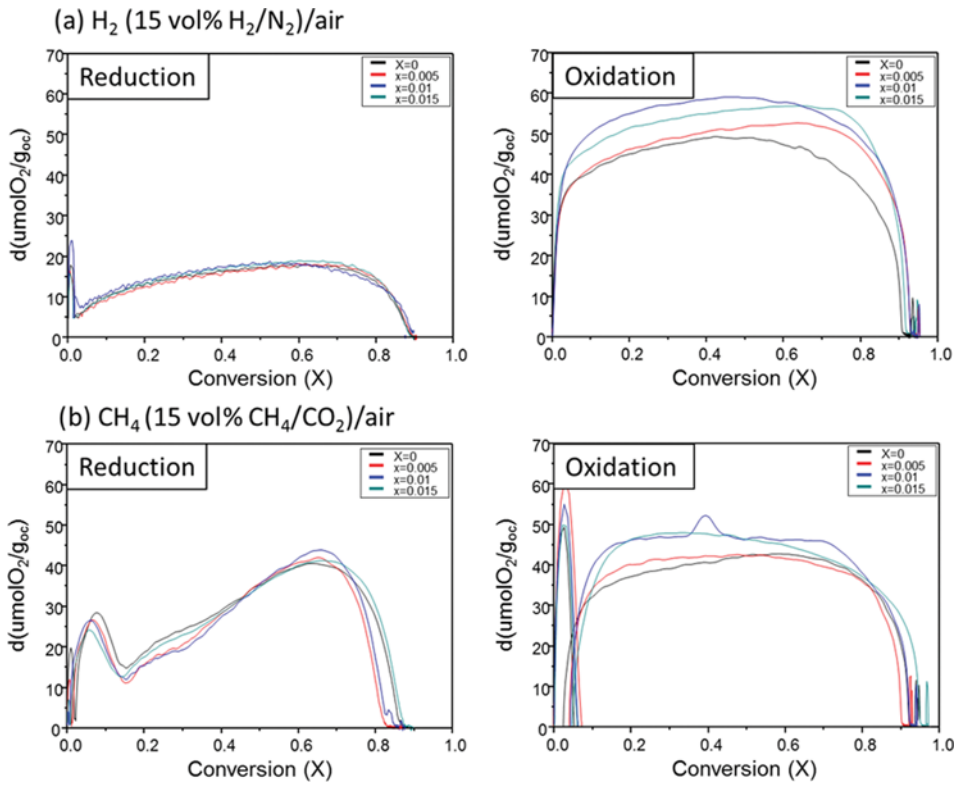


**Fig. 8. The conversion and oxygen transfer rates of reduction and oxidation for (a) $H_2$ (15 vol%$H_2$/$N_2$)/air and (b) $CH_4$ (15 vol% $CH_4$/$CO_2$)/air on the $Ca_{1-x}Li_xMnO_3$ particles.**

and the 40 μmol $O_2/g_{oc}$ oxygen transfer rate presented a conversion of over 0.6. This is considered to be because four oxygen atoms were used to convert 1 mol of $CH_4$ to $CO_2$ and $2H_2O$. In the oxidation reaction, similar reaction trends were observed for the $H_2$ and $CH_4$ atmospheres, and the reaction rate increased as the amount of Li increased. It is considered that the Mn oxidation was effected

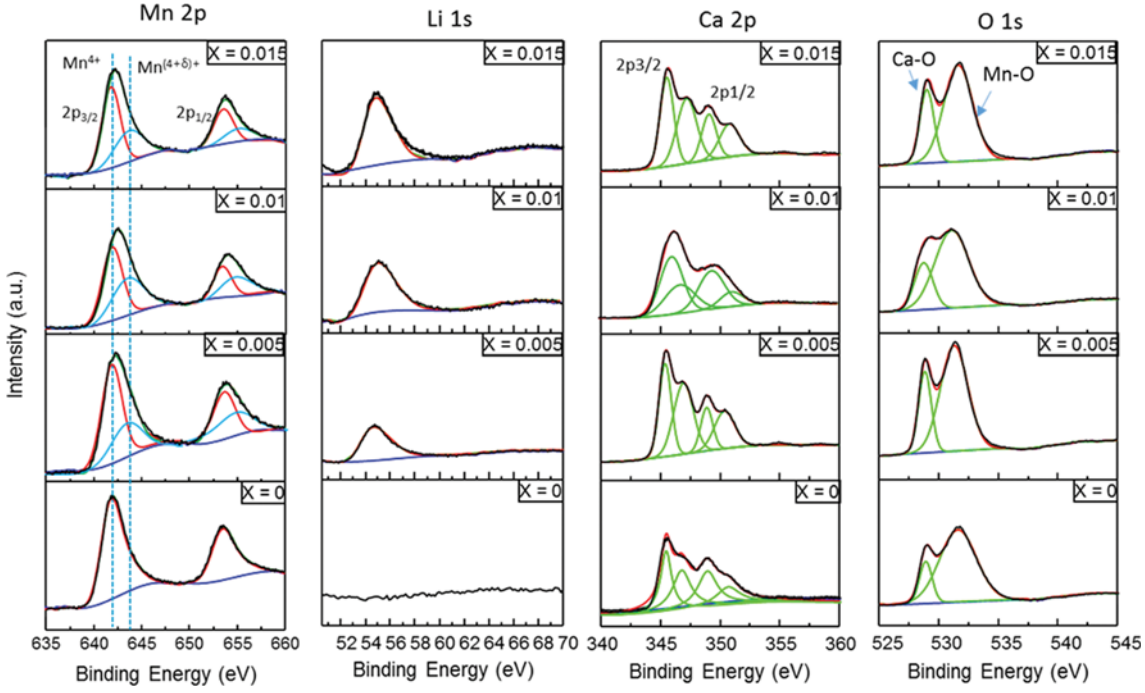


**Fig. 9. The XPS curves for the Ca2p, Li1s, Mn2p and O1s in the $Ca_{1-x}Li_xMnO_3$ particles.**

**Table 2. The Roc,t value of the last cycle of $Ca_{1-x}Li_xMnO_3$ particles and surface area of particles**

(wt%)

| Condition | $CaMnO_3$ | $Ca_{0.995}Li_{0.005}MnO_3$ | $Ca_{0.99}Li_{0.01}MnO_3$ | $Ca_{0.085}Li_{0.015}MnO_3$ |
|---|---|---|---|---|
| $H_2$/air | 8.25 | 8.27 | 8.47 | 8.29 |
| $CH_4$/air | 8.29 | 8.45 | 8.78 | 8.44 |

by Li, which is a strong oxidizing agent.

The XPS spectra of the $Ca_{1-x}Li_xMnO_3$ particles were measured to determine the oxidation state of the elements based on their chemical bonds (results are shown in Fig. 9). The main Ca $2p_{3/2}$, Mn $2p_{3/2}$, and O 1s peaks were clearly observed in the spectra of the $Ca_{1-x}Li_xMnO_3$ particles, and the Li 1s peak intensity increased as the amount of Li was increased. The binding energies of Li 1s, Ca $2p_{3/2}$ and Mn $2p_{3/2}$ were 54.98, 345.48 and 642.18 eV, which were assigned to be $Li^+$, $Ca^{2+}$ and $Mn^{4+}$, respectively. The Mn $2p_{3/2}$ and $2p_{1/2}$ peaks were confirmed at a binding energy of 642.18 eV and 653.78 eV, respectively. These peaks were shifted to higher binding energies as the amount of added Li was increased. When deconvolution work was performed, two peaks were observed at 641.80 and 644.27 eV. The peak at 641.80 eV corresponds to $Mn^{4+}$ because it appears at the same position as $Mn_{2p}$ of $CaMnO_3$ which is Li-free particle and the peak at 644.27 eV corresponds to $Mn^{(4+\delta)+}$ more oxidized. Comparing the areas of the two peaks, the $Mn^{(4+\delta)+}$/$Mn^{4+}$ of X=0.005, 0.01 and 0.015 were 0.58, 1.20 and 0.63, respectively. This analysis confirms that the amount of Mn with a high oxidation state at X=0.01 particle was more than other particles. The results indicate that the oxidation state of Mn in the $CaMnO_3$ perovskite structure was increased as a result of using Li to substitute Ca sites. The high oxidation state of Mn means that it can contain more oxygen, which is a factor considered to have an important effect on the improved performance of the synthesized particles. In addition, two $O_{1s}$ peaks were found in the spectra, and the peaks at 531.68 eV and 528.98 eV were assigned to the oxygen of Ca-O [27] and Mn-O [28], respectively. Table 1 is the result of quantitative analysis. Ca and Mn were present in a ratio of about 1 : 1, and the contents varied depending on the amounts of Li and Ca added.

## CONCLUSIONS

We investigated the effect of the oxidation state of Mn on CLC reactions. This was achieved by replacing Ca with Li in $Ca_{1-x}Li_xMnO_3$ particles to increase the oxidation state of Mn and thus improve the oxygen transfer performance of the particles under $H_2$ and $CH_4$ atmospheres. The synthesized $Ca_{1-x}Li_xMnO_3$ particles presented a $CaMnO_3$ perovskite structure; therefore, Li was stably and well substituted at the Ca site of the $CaMnO_3$ perovskite structure. XPS analysis results confirmed that the addition of Li affected the oxidation state of Mn in $CaMnO_3$. Corresponding to these analytical results, the oxygen transfer performance of the $Ca_{1-x}Li_xMnO_3$ particles was higher than that of $CaMnO_3$. Particularly, the $Ca_{0.99}Li_{0.01}MnO_3$ particles presented the highest performance of 8.47 and 8.78 wt%, under $H_2$-$N_2$/air and $CH_4$-$CO_2$/air conditions, respectively. Through this study, it was confirmed that the change of the oxidation state of the active metal is an important factor to improve the performance of oxygen carrier particles in CLC reactions.

## ACKNOWLEDGEMENTS

This work was supported by the Energy Efficiency & Resources Programs of the Korea Institute of Energy Technology Evaluation and Planning (KETEP), granted financial resources from the Ministry of Trade, Industry & Energy, Republic of Korea (20152010201840).

## REFERENCES

1. W. L. Theo, J. S. Lim, H. Hashim, A. A. Mustaffa and W. S. Ho, *Appl. Energy*, **183**, 1633 (2016).
2. Z. Dai and L. Deng, *Int. J. Greenhouse Gas Control*, **54**, 59 (2016).
3. K. Mezghani and A. Hamza, *J. Membr. Sci.*, **518**, 254 (2016).
4. S. Niu, M. Chen, Y. Li and F. Xue, *Fuel*, **178**, 129 (2016).
5. M. Vaccarelli, M. Sammak, K. Jonshagen, R. Carapellucci and M. Genrup, *Energy*, **112**, 917 (2016).
6. T. Zarogiannis, A. I. Papadopoulos and P. Seferlis, *J. Cleaner Prod.*, **136**, 159 (2016).
7. J.-H. Choi, P. S. Youn, D. Brahimi, Y.-W. Jeon, S. D. Kim and H.-J. Ryu, *Korean J. Chem. Eng.*, **29**, 737 (2012).
8. A. Nandy, C. Loha, S. Gu, P. Sarkar, M. K. Karmakar and P. K. Chatterjee, *Renewable Sustainable Energy Rev.*, **59**, 597 (2016).
9. L. Protasova and F. Snijkers, *Fuel*, **181**, 75 (2016).
10. M. Johansson, T. Mattisson and A. Lyngfelt, *Chem. Eng. Res. Des.*, **84**, 807 (2006).
11. S. Bhavsar, B. Tackett and G. Veser, *Fuel*, **136**, 268 (2014).
12. K. Svoboda, A. Siewiorek, D. Baxter, J. Rogut and M. Pohorelý, *Energy Convers. Manage.*, **49**, 221 (2008).
13. J.-I. Baek, C. K. Ryu, J. H. Lee, T. H. Eom, J. B. Lee, H.-J. Ryu, J. Ryu and J. Yi, *Fuel*, **102**, 106 (2012).
14. W. S. Song, Y. S. Seo, H. K. Yoon and S. J. Cho, *Korean J. Chem. Eng.*, **20**, 471 (2003).
15. L. F. de Diego, P. Gayán, F. García-Labiano, J. Celaya, A. Abad and J. Adánez, *Energy Fuels*, **19**, 1850 (2005).
16. B. S. Kwak, N.-K. Park, J.-I. Baek, H.-J. Ryu and M. Kang, *Powder Technol.*, **312**, 237 (2017).
17. Z.-F. Gao, Z.-J. Wu and W.-M. Liu, *J. Environ. Chem. Eng.*, **4**, 1653 (2016).
18. Q. Imtiaz, M. Broda and C. R. Müller, *Appl. Energy*, **119**, 557 (2014).
19. Y. Zhang, E. Doroodchi and B. Moghtaderi, *Appl. Energy*, **113**, 1916 (2014).
20. B. S. Kwak, N.-K. Park, S. O. Ryu, J.-I. Baek, H.-J. Ryu and M. Kang, *Chem. Eng. J.*, **309**, 617 (2017).
21. M. Wang, J. Liu, F. Shen, H. Hao, J. Dai and Y. Long, *Appl. Surf. Sci.*, **367**, 485 (2016).
22. P. Hallberg, M. Rydén, T. Mattisson and A. Lyngfelt, *Energy Procedia*, **63**, 80 (2014).

23. N. Galinsky, M. Sendi, L. Bowers and F. Li, *Appl. Energy*, **174**, 80 (2016).
24. N. Galinsky, A. Mishra, J. Zhang and F. Li, *Appl. Energy*, **157**, 358 (2015).
25. A. Abad, F. García-Labiano, P. Gayán, L. F. de Diego and J. Adánez, *Chem. Eng. J.*, **269**, 67 (2015).
26. P. Gayán, I. Adánez-Rubio, A. Abad, L. F. de Diego, F. Garía-Labiano and J. Adánez, *Fuel*, **96**, 226 (2012).
27. R. Koirala, K. R. Gunugunuri, S. E. Pratsinis and P. G. Smirniotis, *J. Phys. Chem. C.*, **115**, 24804 (2011).
28. Z. Li, J. Wang, X. Liu, S. Liu, J. Ou and S. Yang, *J. Mater. Chem.*, **21**, 3397 (2011).